International Journal of Heat and Mass Transfer 79 (2014) 1027–1033

Contents lists available at ScienceDirect

International Journal of Heat and Mass Transfer

journal homepage: www.elsevier.com/locate/ijhmt

Analytical modeling of temperature distribution in an anisotropic cylinder with circumferentially-varying convective heat transfer

D. Sarkar, K. Shah, A. Haji-Sheikh, A. Jain *

Mechanical and Aerospace Engineering Department, University of Texas at Arlington, TX, USA

ARTICLE INFO

Article history:
Received 19 March 2014
Received in revised form 21 August 2014
Accepted 22 August 2014

Keywords:
Convective heat transport
Cross flow over a cylinder
Thermal modeling
Anisotropic thermal conduction
Li-ion batteries

ABSTRACT

Fluid flow past a cylinder is a classical problem of fluid mechanics and convective heat transfer. In this problem, the local convective heat transfer coefficient on the cylinder surface varies around the cylinder due to boundary layer growth, separation and transition to turbulence. While there is considerable literature on computing the temperature distribution in the fluid, not much work exists on computing the temperature distribution within the solid body, particularly if the solid has anisotropic thermal properties. This paper presents an analytical technique for computing the temperature distribution within a heat-generating cylinder with anisotropic thermal conductivity subjected to spatially varying convective heat transfer coefficient due to fluid flow. As expected, temperature distribution on the cylinder surface exhibits minima and maxima at locations where the convective heat transfer coefficient has maxima and minima respectively. The effect of various parameters, including Reynolds number of the flow and extent of anisotropy are examined. Results presented in this paper contribute towards the fundamental understanding of a classical heat transfer problem. Further, since Li-ion cells that are commonly used for energy conversion and storage exhibit strong thermal conduction anisotropy, these results may be useful for design of convection-based thermal management of Li-ion cells.

1. Introduction

Convective heat transfer between a solid body and fluid flow past the body is an important technological problem for which a vast amount of literature on experimental investigation as well as theoretical modeling exists [1,2]. For fluid flow past a solid body, the convective heat transfer coefficient, h, at the surface of the body is known to vary spatially. For the specific case of flow past a cylinder, the variation of h as a function of the circumferential angle, θ is well known. This variation has been experimentally measured for different values of Reynolds number, Re [2], and has also been computed by solving the governing energy and momentum conservation equations of the flow [3]. Starting from the stagnation point ($\theta = 0°$), h first decreases due to laminar boundary layer development. For laminar flow, a minima is reached at around $\theta = 80°$ where separation occurs. For large values of Re, a sharp increase occurs beyond the first minima due to transition to turbulence, following which a second minima occurs due to separation at around $\theta = 140°$. Mixing in the wake region results in further increase in h beyond this minima [1]. For the case of flow past a cylinder, the temperature and velocity fields in the flow around the cylinder have been computed theoretically and analytically. However, not much work exists that addresses the computation of temperature within the cylinder while accounting for the θ-dependence of h. The problem of variable convective heat transfer coefficient occurs commonly in the thermal analysis of extended surfaces [4]. This problem has been analyzed in a number of papers. Steady state temperature distribution for a one dimensional rectangular fin with temperature-dependent heat transfer coefficient has been presented [5]. A solution method to determine temperature involving direct integration of the governing differential equation has been presented [6]. A method based on Fourier series expansion has been adopted to determine the two-dimensional temperature field in a rectangular fin in which the heat transfer coefficient varies along the length of the fin [7]. Another paper analyzes the variable heat transfer coefficient problem for computing temperature in the thermal entry region of a hydrodynamically developed duct flow [8]. The Frobenius series expansion technique has been used for fins with different cross-sectional areas with varying heat transfer coefficients [9]. Another paper highlights the performance of annular fins of different profiles when subjected to variable heat transfer coefficient [10].

* Corresponding author. Address: 500W First St, Rm 211, Arlington, TX 76019, USA. Tel.: +1 (817) 272 9338; fax: +1 (817) 272 2952.
E-mail address: jaina@uta.edu (A. Jain).

http://dx.doi.org/10.1016/j.ijheatmasstransfer.2014.08.060
0017-9310/

Nomenclature

h	convective heat transfer coefficient over curved surface of the cylinder	k_θ	circumferential thermal conductivity
h_{end}	convective heat transfer coefficient over end surfaces of the cylinder	k_z	axial thermal conductivity
H	cylinder height	Q	heat generation rate
k_r	radial thermal conductivity	R	cylinder radius
		T	temperature rise above ambient

Semi-analytical solution methods such as the Galerkin based integral method has also been adopted to account for variable heat transfer coefficient in fins [11]. An inverse problem that estimates the functional form of the heat flux at the base of the fin when the surface of the fin is subjected to variable heat transfer coefficient has been presented [12]. Another paper has addressed the inverse problem of computing the space dependent heat transfer coefficient when temperature at certain locations inside the body at certain locations is known a priori [13]. A hybrid numerical scheme has been used for transient thermo-elastic analysis of an annular fin with [14]. Numerical analysis has also been carried out for determining the transient natural convective heat transfer with variable heat transfer coefficient in the case of domestic refrigerators [15]. The literature cited above indicates that the variable heat transfer coefficient problem has been adequately addressed for extended surfaces. However, there is a lack of literature for addressing variable heat transfer coefficient in the context of cross flow past a solid cylinder, a problem of considerable technological importance. This is particularly so when thermal conduction inside the cylinder is anisotropic in nature. Recent research on Li-ion batteries suggests the existence of strong anisotropy in thermal conduction in Li-ion cells [16]. Thermal conductivity measurements indicate a 100-fold difference in thermal conductivity in the radial and axial directions [16]. The cooling of Li-ion cells is a problem of much technological importance [17]. Li-ion cells are commonly used for energy storage and conversion, and thermal runaway is a significant problem in insufficiently cooled Li-ion cells, which in extreme cases leads to explosion and fire, as evidenced in recent incidents on aircrafts [18]. As a result, it is important to develop analytical techniques for computing the temperature of a Li-ion cells that account for the anisotropic nature of thermal conduction within the cell, and also the variable convective heat transfer coefficient around the cell that may occur due to flow of a coolant fluid past the cell.

This paper presents an analytical technique to compute the temperature profile within an infinite or a finite cylinder subjected to internal heat generation and a convective heat transfer coefficient on the outer surface that varies around the cylinder in the θ direction. The analytical model results in a series solution for the temperature profile with coefficients that can be computed easily by solving a well-defined set of linear algebraic equations.

Using the functional form of $h(\theta)$ from well-known experiments, [1,2], the expected temperature profile is computed for a cylinder subjected to an external coolant flow. The dependence of the temperature profile on a number of parameters such as the Reynolds number of the external flow, extent of thermal conduction anisotropy, aspect ratio, etc. is discussed. In addition to addressing a classical theoretical problem, this paper may also help develop design tools for thermal management of Li-ion cells using external coolant flow.

2. Analytical model

Consider the steady state thermal conduction problem of a heat-generating cylinder of radius R subjected to circumferentially varying convective heat transfer on its outer surface, represented by $h(\theta)$. Note that $h(\theta)$ must be an even function and periodic with a period of 2π. A uniform volumetric heat generation rate Q is assumed to occur within the cylinder. Two specific cases shown in Fig. 1(a) and (b) are considered – an infinitely long cylinder, and a finite cylinder of height H. The finite cylinder is subjected to a constant convective heat transfer coefficient h_{end} at the top and bottom surfaces. Thermal conduction within the cylinder is assumed to be anisotropic, with the radial, circumferential and axial thermal conductivities given by k_r, k_θ and k_z, respectively. Such anisotropy occurs, for example, in a Li-ion battery in which recent experimental measurements have indicated a 100-fold difference in the axial and radial thermal conductivities [16]. The primary interest in this paper is to derive an analytical expression for the temperature distribution $T(r,\theta)$ for the infinite cylinder, and $T(r,\theta,z)$ for the finite cylinder.

2.1. Infinite cylinder

In this case, the governing energy equation is given by

$$\frac{k_r}{r}\frac{\partial}{\partial r}\left(r\frac{\partial T}{\partial r}\right)+\frac{k_\theta}{r^2}\frac{\partial^2 T}{\partial \theta^2}+Q=0 \tag{1}$$

where $T(r,\theta)$ is the temperature rise above ambient.

The temperature distribution is subject to the following boundary conditions:

$$\frac{\partial T}{\partial r}=0 \quad \text{at } r=0 \tag{2}$$

$$k_r\frac{\partial T}{\partial r}+h(\theta)\cdot T=0 \quad \text{at } r=R \tag{3}$$

$$T(\theta)=T(\theta+2\pi) \tag{4}$$

$$\left.\frac{\partial T}{\partial \theta}\right|_{\theta}=\left.\frac{\partial T}{\partial \theta}\right|_{\theta+2\pi} \tag{5}$$

Eq. (2) is based on the requirement of symmetry of the temperature field about $r = 0$. Eq. (3) represents circumferentially varying convective heat transfer at the outer surface, $r = R$. Eqs. (4) and (5) arise from temperature and heat flux periodicity in the circumferential direction.

Eqs. (1)–(5) represent a thermal conduction problem in which the governing energy equation is non-homogeneous, whereas all boundary conditions are homogeneous. If the convective heat transfer coefficient in Eq. (3) were to be constant, this set of equations admits a straightforward solution using the separation of variables approach. However, θ-dependence of h precludes this approach. Instead, a more general approach that accounts for θ-dependence of h must be adopted. The temperature field is first split into two parts as follows:

$$T(r,\theta)=w(r,\theta)-\frac{Q\,r^2}{4k_r} \tag{6}$$

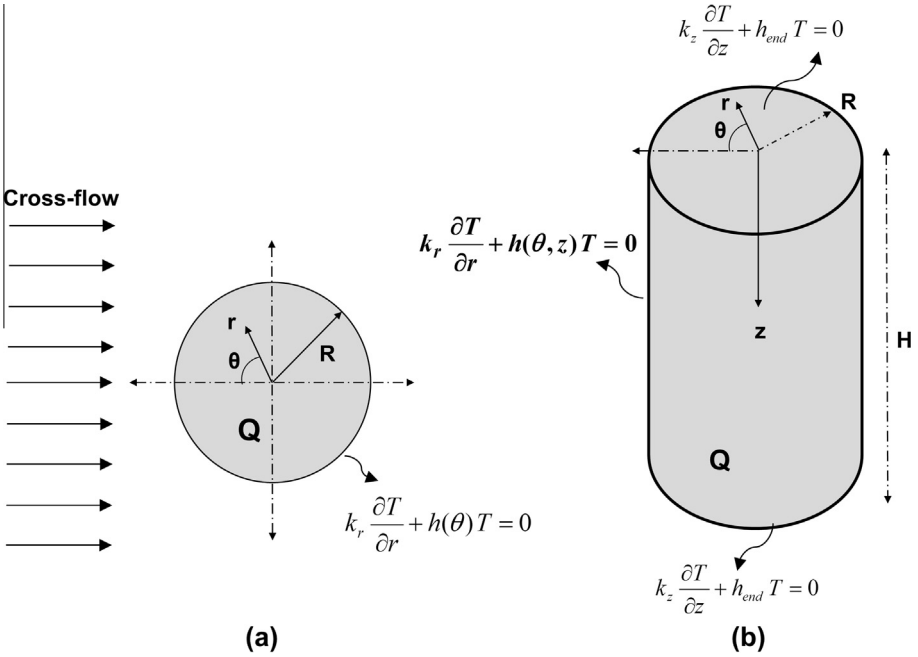

Fig. 1. Schematic of the geometry under consideration for (a) infinite, and (b) finite cylinder subjected to circumferentially varying convection at the surface due to cross-flow.

Splitting of the temperature field in this manner results in a homogeneous governing equation for $w(r,\theta)$, with one non-homogeneous boundary condition at $r = R$, as follows:

$$\frac{k_r}{r}\frac{\partial}{\partial r}\left(r\frac{\partial w}{\partial r}\right) + \frac{k_\theta}{r^2}\frac{\partial^2 w}{\partial \theta^2} = 0 \tag{7}$$

subject to

$$\frac{\partial w}{\partial r} = 0 \quad \text{at } r = 0 \tag{8}$$

$$k_r \frac{\partial w}{\partial r} + h(\theta) w = F(\theta) \quad \text{at } r = R \tag{9}$$

$$w(\theta) = w(\theta + 2\pi) \tag{10}$$

$$\left.\frac{\partial w}{\partial \theta}\right|_{\theta} = \left.\frac{\partial w}{\partial \theta}\right|_{\theta+2\pi} \tag{11}$$

where

$$F(\theta) = \frac{QR}{2}\left[1 + \frac{h(\theta)R}{2k_r}\right] \tag{12}$$

The boundary conditions in Eqs. (7)–(12) are all homogeneous, except one. The solution for $w(r,\theta)$ is written in terms of an infinite series as follows:

$$w(r,\theta) = \sum_{m=0}^{\infty} C_m \cos(m\theta)\left(\frac{r}{R}\right)^{m\sqrt{k_\theta/k_r}} \tag{13}$$

Eq. (13) already satisfies the governing differential equation given by Eq. (7) and three boundary conditions given by Eqs. (8), (10) and (11). The coefficients C_m in Eq. (13) can be chosen in a manner so as to satisfy the last remaining boundary condition, given by Eq. (9). To do so, $w(r,\theta)$ from Eq. (13) is inserted in Eq. (9), resulting in

$$k_r \sum_{m=0}^{\infty} C_m \cos(m\theta)\frac{m\sqrt{k_\theta/k_r}}{R} + h(\theta)\sum_{m=0}^{\infty} C_m \cos(m\theta) = F(\theta) \tag{14}$$

Finally, Eq. (14) is multiplied by $\cos(j\theta)$ and integrated from $\theta = 0$ to $\theta = 2\pi$. Because h is a function of θ, this results in a set of linear equations involving the unknown coefficients:

$$C_j b_j + \sum_{m=0}^{\infty} C_m d_{j,m} = f_j \quad \text{for each } j = 0,1,2,3,4\ldots \tag{15}$$

where

$$b_j = \frac{j\sqrt{k_r k_\theta}}{R}\int_{\theta=0}^{2\pi} \cos^2(j\theta)\, d\theta \tag{16}$$

$$d_{j,m} = \int_0^{2\pi} h(\theta)\cos(j\theta)\cos(m\theta)d\theta \tag{17}$$

$$f_j = \int_0^{2\pi} F(\theta)\cos(j\theta)d\theta \tag{18}$$

Assuming that the maximum value of m in Eq. (14) is M, Eq. (15) represents a set of $(M+1)$ linear equations in $(M+1)$ unknowns C_j, $j = 0,1,2,\ldots,M$, from where the unknown coefficients can be computed. Once the coefficients are computed, Eqs. (6) and (13) represent the temperature distribution in the anisotropic cylinder. Putting $k_r = k_\theta$ in equations above reduces the solution to that for an isotropic cylinder with identical thermal conductivity in each direction.

It is to be noted that in the special case of h being independent of θ, $d_{j,m}$ become zero except when $j = m$. As a result, Eq. (15) reduces to $(b_j + d_{j,j})\cdot C_j = f_j$, from where all C_j's can be obtained explicitly without the need to solve a set of algebraic equations. This corresponds to the separation of variables approach for constant h, in which all coefficients can be obtained explicitly, as opposed to the case considered here, where the coefficients are determined through the solution of a set of linear algebraic equations.

2.2. Finite cylinder of height H

This sub-section considers a finite cylinder of height H. In this case, the governing energy equation is given by

$$\frac{k_r}{r}\frac{\partial}{\partial r}\left(r\frac{\partial T}{\partial r}\right)+\frac{k_\theta}{r^2}\frac{\partial^2 T}{\partial \theta^2}+k_z\frac{\partial^2 T}{\partial z^2}+Q=0 \tag{19}$$

The temperature field $T(r, \theta, z)$ satisfies the boundary conditions given by Eqs. (2)–(5). Note that the convective heat transfer coefficient in Eq. (3) is now a function of θ as well as z, i.e. $h = h(\theta,z)$. The temperature field also satisfies the following boundary conditions in the z direction:

$$k_z\frac{\partial T}{\partial z}-h_{end}\cdot T=0 \quad \text{at } z=0 \tag{20}$$

and

$$k_z\frac{\partial T}{\partial z}+h_{end}\cdot T=0 \quad \text{at } z=H \tag{21}$$

In this case, the solution methodology is similar to that described for the infinite cylinder in Section 2.1. The solution is given by

$$T(r,\theta,z)=w(r,\theta,z)+f(z) \tag{22}$$

where

$$f(z)=\frac{QH^2}{2k_z}\left(\frac{z}{H}\left(1-\frac{z}{H}\right)+\frac{1}{Bi}\right) \tag{23}$$

and $Bi=\frac{h_{end}\cdot H}{k_z}$.

The governing equation for $w(r, \theta, z)$ is

$$\frac{k_r}{r}\frac{\partial}{\partial r}\left(r\frac{\partial w}{\partial r}\right)+\frac{k_\theta}{r^2}\frac{\partial^2 w}{\partial \theta^2}+k_z\frac{\partial^2 w}{\partial z^2}=0 \tag{24}$$

$w(r,\theta,z)$ satisfies the boundary conditions given by Eqs. (8), (10), (11). In addition, w also satisfies

$$k_z\frac{\partial w}{\partial z}-h_{end}\cdot w=0 \quad \text{at } z=0 \tag{25}$$

$$k_z\frac{\partial w}{\partial z}+h_{end}\cdot w=0 \quad \text{at } z=H \tag{26}$$

and

$$-k_r\left.\frac{\partial w}{\partial r}\right|_{r=R}=h(\theta,z)\cdot(w+f(z)) \tag{27}$$

Using an approach similar to Section 2.1, $w(r,\theta,z)$ may be written as

$$w(r,\theta,z)=\sum_{m=0}^{\infty}\sum_{n=1}^{\infty}C_{mn}\cdot I_{\upsilon_m}\left(\eta_n\sqrt{\frac{k_z}{k_r}}r\right)\cos(m\theta)\left[\frac{h_{end}}{\eta_n k_z}\sin(\eta_n z)+\cos(\eta_n z)\right] \tag{28}$$

where I is the modified Bessel function of the first kind. The order of the Bessel function is given by

$$\upsilon_m=m\sqrt{\frac{k_\theta}{k_r}} \tag{29}$$

The eigenvalues η_n are determined from roots of the equation

$$\tan(\eta_n H)=\frac{2(\eta_n\cdot H)Bi}{(\eta_n\cdot H)^2-Bi^2} \tag{30}$$

The solution form shown in Eq. (28), when substituted in the boundary condition at $r = R$, given by Eq. (27) results in

$$\begin{aligned}&k_r\eta_n\sqrt{\frac{k_z}{k_r}}\sum_{m=0}^{\infty}\sum_{n=1}^{\infty}C_{mn}\left[\frac{m}{\eta_n R}\sqrt{\frac{k_\theta}{k_z}}\cdot I_{\upsilon_m}\left(\eta_n\sqrt{\frac{k_z}{k_r}}R\right)+I_{\upsilon_m+1}\left(\eta_n\sqrt{\frac{k_z}{k_r}}R\right)\right]\\&\times\cos(m\theta)\left[\frac{h_{end}}{\eta_n k_z}\sin(\eta_n z)+\cos(\eta_n z)\right]+\sum_{m=0}^{\infty}\sum_{n=1}^{\infty}C_{mn}h(\theta,z)\cdot I_{\upsilon_m}\\&\times\left(\eta_n\sqrt{\frac{k_z}{k_r}}R\right)\cos(m\theta)\left[\frac{h_{end}}{\eta_n k_z}\sin(\eta_n z)+\cos(\eta_n z)\right]=-h(\theta,z)f(z)\end{aligned} \tag{31}$$

Using a similar approach as shown in Section 2.1 following Eq. (14), use of orthogonality in Eq. (31) results in a set of linear equations involving the unknown coefficients given by

$$C_{ji}\,b_{ji}+\sum_{m=0}^{\infty}\sum_{n=1}^{\infty}C_{mn}\,d_{jimn}=f_{ji} \tag{32}$$

where

$$b_{ji}=\eta_i\sqrt{k_z k_r}\left[\frac{j}{\eta_i R}\sqrt{\frac{k_\theta}{k_z}}\cdot I_{\upsilon_j}\left(\eta_i\sqrt{\frac{k_z}{k_r}}R\right)+I_{\upsilon_j+1}\left(\eta_i\sqrt{\frac{k_z}{k_r}}R\right)\right]N_\theta N_z \tag{33}$$

$$\begin{aligned}d_{jimn}=&I_{\upsilon_m}\left(\eta_n\sqrt{\frac{k_z}{k_r}}R\right)\times\int_0^H\int_0^{2\pi}h(\theta,z)\cos(m\theta)\\&\times\cos(j\theta)\left[\frac{h_{end}}{\eta_n k_z}\sin(\eta_n z)+\cos(\eta_n z)\right]\left[\frac{h_{end}}{\eta_i k_z}\sin(\eta_i z)+\cos(\eta_i z)\right]d\theta dz\end{aligned} \tag{34}$$

$$f_{ji}=-\int_0^H\int_0^{2\pi}h(\theta,z)f(z)\cos(j\theta)\left[\frac{h_{end}}{\eta_i k_z}\sin(\eta_i z)+\cos(\eta_i z)\right]d\theta dz \tag{35}$$

The norms N_θ and N_z in Eq. (33) are given by [19]

$$N_\theta=\int_0^{2\pi}\cos^2(j\theta)d\theta=\begin{cases}2\pi & \text{when } j=0\\ \pi & \text{when } j\neq 0\end{cases} \tag{36}$$

$$\begin{aligned}N_z&=\int_0^H\left[\frac{h_{end}}{\eta_i k_z}\sin(\eta_i z)+\cos(\eta_i z)\right]^2dz\\&=\left(\frac{h_{end}^2}{(\eta_i k_z)^2}+1\right)\frac{H}{2}+\frac{h_{end}}{k_z\eta_i^2}\end{aligned} \tag{37}$$

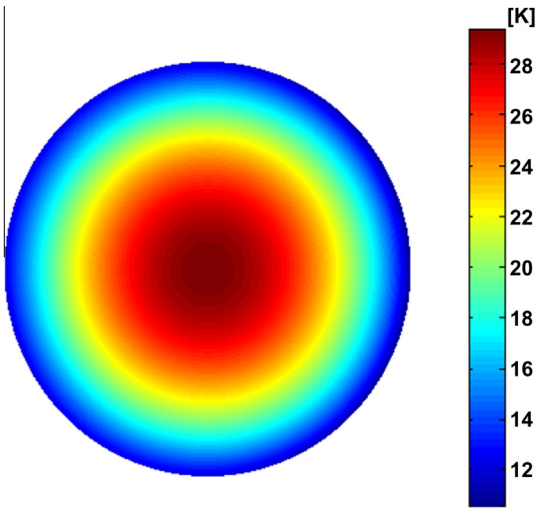

Fig. 2. Polar plot of the temperature distribution in an anisotropic infinite cylinder at $Re = 7960$.

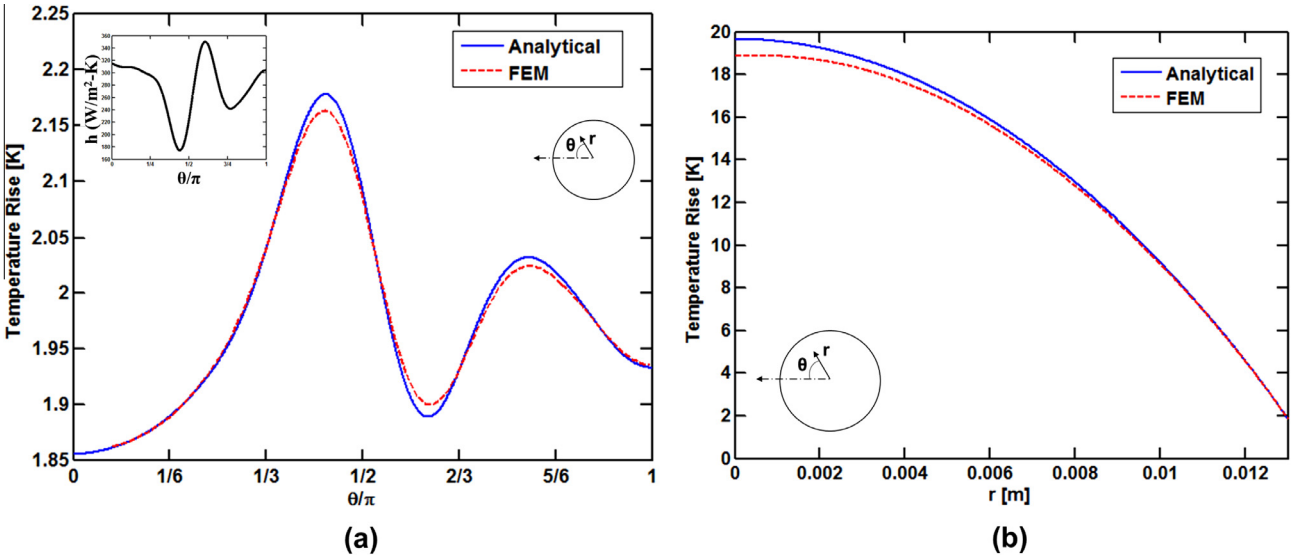

Fig. 3. Comparison of the analytically computed temperature distribution for the infinite cylinder with finite-element modeling results. (a) Shows variation with θ, (b) shows variation with r.

Solving the set of linear algebraic equations involving the coefficients C_{mn} given by Eq. (32) results in the determination of the temperature distribution for the finite cylinder given by Eq. (22). Note that the ratios of various thermal conductivities appearing in the solution account for the thermal conduction anisotropy in the cylinder. Putting $k_r = k_\theta = k_z$ results in a solution for the isotropic cylinder.

3. Results and discussion

Fig. 2 presents a polar plot of temperature distribution in an infinite cylinder of radius 13 mm with $Re = 7960$ computed using the model in Section 2.1. The θ-variation of h is obtained from well-known experimental data [2]. Radial and circumferential thermal conductivities are assumed to be $k_r = 0.2$ W/mK and $k_\theta = 30$ W/mK, respectively, based on recent measurements on a 26650 Li-ion cell [16]. While the θ-variation in the temperature distribution shown in Fig. 2 may not be readily apparent due to the much larger radial variation, it is clearly seen in Fig. 3, which presents line plots of temperature distribution as a function of θ at the outer surface (Fig. 3(a)), and as a function of r (Fig. 3(b)). Inset in Fig. 3(a) shows the variation of h as a function of theta. Fig. 3(a) and (b) also present the temperature distributions predicted by a finite-element simulation. Similar plots are presented for a finite-cylinder at the mid-height in Fig. 4(a) and (b). For the finite cylinder case, a cylinder of radius 13 mm and height 65 mm is used, which corresponds to the geometry of the commonly used 26650 Li-ion cell. Figs. 3 and 4 show that the infinite cylinder and finite cylinder models are both in excellent agreement with finite-element simulation results. The temperature field is found to have maxima and minima at θ locations where the distribution of the heat transfer coefficient has minima and maxima respectively. This is along expected lines since a large value of the local convective heat transfer coefficient results in greater local heat transfer from the solid to the fluid, and thus lower solid temperature. While the model predictions and finite-element simulation results are within less than 1% of each other for most of the cylinder, the maximum deviation between the two is about 3%, which occurs at the temperature peaks. This small error occurs possibly due to approximations related to the number of eigenvalues used in the model, and due to numerical errors in computing the integrals present in the model. Additionally,

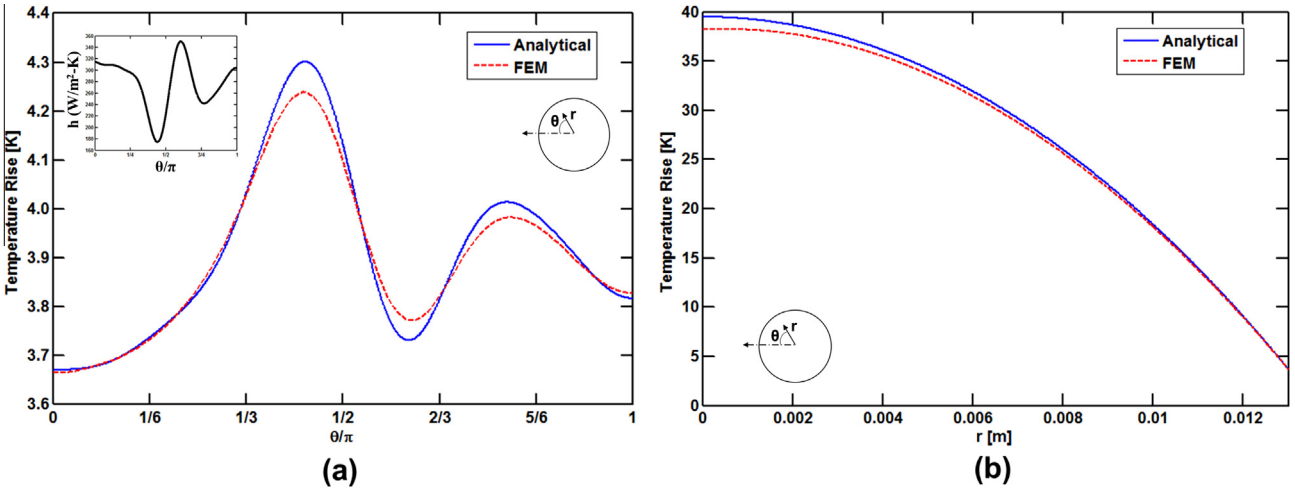

Fig. 4. Comparison of the analytically computed temperature distribution for the finite cylinder at mid-height with finite-element modeling results. (a) Shows variation with θ, (b) shows variation with r.

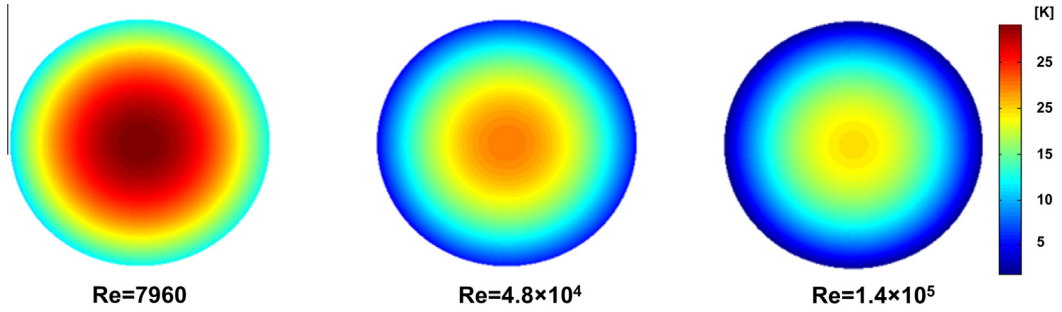

Fig. 5. Polar plots for the temperature distribution in an anisotropic infinite cylinder with three different values of Reynolds number, with k_r = 0.2 W/mK, k_θ = 30 W/mK based on recent measurements [16].

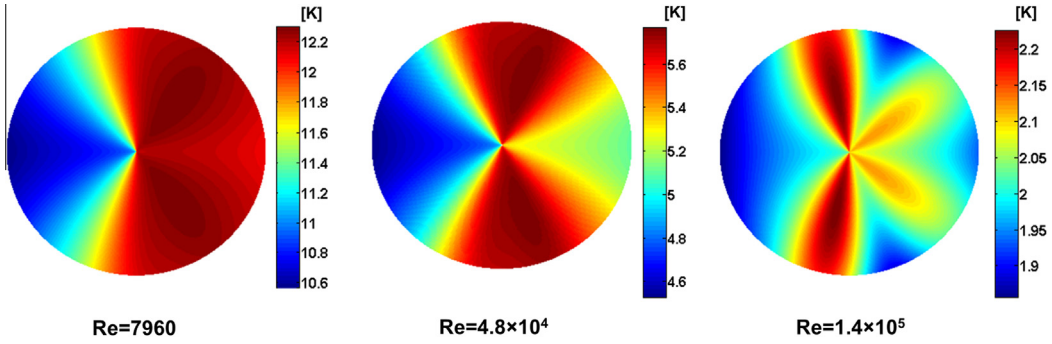

Fig. 6. Polar plots for the temperature distribution in an anisotropic infinite cylinder with three different values of Reynolds number, with k_r = 30 W/mK, k_θ = 0.2 W/mK.

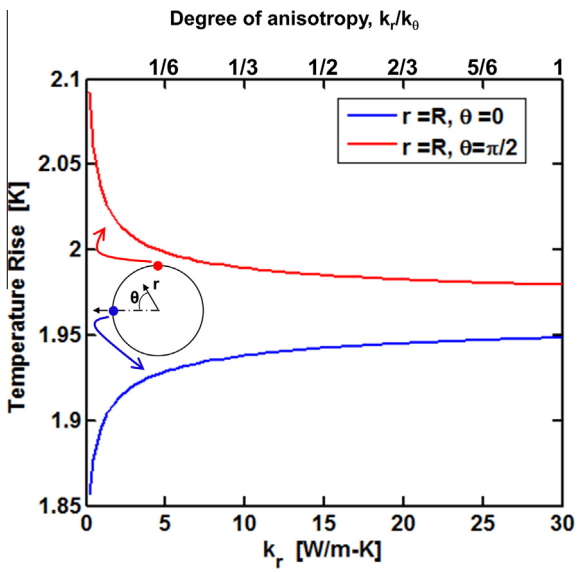

Fig. 7. Plot of temperature rise as a function of the degree of thermal conduction anisotropy in an infinite cylinder.

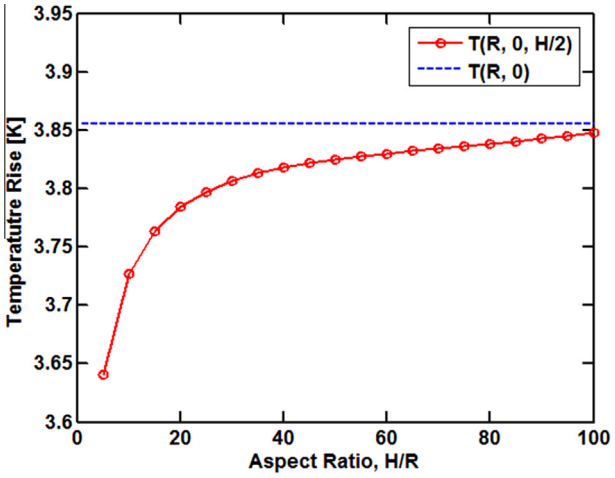

Fig. 8. Plot of temperature as a function of aspect ratio for a finite cylinder.

approximations in the finite-element simulation may also have contributed to the small error.

The model presented in Section 2 is next used to determine the temperature distribution within the cylinder for different values of *Re*. Well-known measurements of the convective heat transfer coefficient on the cylinder surface as a function of θ at various values of *Re* [2] are used in these computations. Fig. 5 shows polar plots of temperature distribution in the cylinder for three values of *Re*. The thermal properties and heat generation rate are the same as used in Figs. 2 and 3. Fig. 5 shows that as *Re* increases, the temperature field within the cylinder reduces, as expected. In addition, these polar plots also demonstrate the radial and circumferential variations in the temperature field within the cylinder. As expected, the core of the cylinder is the hottest in each case, while the outer surface directly facing the fluid flow is the coolest.

In order to illustrate the strong effect of anisotropy in thermal conduction, Fig. 6 shows temperature plots at three values of *Re*, with k_r = 30 W/mK and k_θ = 0.2 W/mK, which is the opposite of the assumption for Fig. 5. In this case, the much lower value of k_θ

relative to k_r is expected to result in significant temperature gradients in the θ direction, which is clearly seen in Fig. 6. Recent measurements on a 26650 Li-ion cell [16] indicate that k_r is expected to be much lower than k_θ, which is why Fig. 5 may be more representative of an actual Li-ion cell than Fig. 6.

In order to further demonstrate the effect of anisotropic thermal conduction, the temperature field in the cylinder is computed as a function of the radial thermal conductivity, while keeping the other thermal conductivities constant. Fig. 7 plots temperature at $\theta = 0°$, and $\theta = 90°$, both at $r = R$ as functions of k_r. The ratio k_r/k_θ, which represents the degree of anisotropy is also indicated. Fig. 7 shows that the temperature at $\theta = 0°$ increases while the temperature at $\theta = 90°$ decreases as k_r increases. At large k_r, the temperatures at the two points converge to the same value, which is along expected lines, since the cylinder will behave as an isothermal body in the limit of large k_r.

Finally, the finite cylinder model is used to compute the temperature distribution in a finite cylinder as a function of aspect ratio H/R, while keeping the volumetric heat generation rate constant. The temperature at the stagnation point at mid-height ($r = R$, $\theta = 0°$, $z = H/2$) is plotted in Fig. 8 as a function of the aspect ratio. Fig. 8 also shows the temperature at this point for an infinite cylinder with the same volumetric heat generation rate and thermal properties. Fig. 8 shows that as the aspect ratio increases, the temperature predicted by the finite model approaches that of the infinite cylinder, since the finite cylinder approaches the limit of an infinite cylinder as the aspect ratio increases.

4. Conclusions

This paper addresses the classical problem of heat transfer between a solid and the cross flow of a cooling fluid. This paper presents an analytical technique to account for spatial variation of h on the cylinder surface predict the temperature field inside the cylinder, particularly if the cylinder has anisotropic thermal properties, as is the case in cylindrical Li-ion cells. The results presented in this paper contribute to the fundamental theoretical understanding of an important heat transfer problem. In addition, the results may also help in understanding heat transfer in energy conversion devices based on Li-ion cells that generate significant heat, and are known to have significant anisotropy in thermal conduction.

References

[1] T.L. Bergman, A.S. Lavine, F.P. Incropera, D.P. DeWitt, Fundamentals of Heat and Mass Transfer, John Wiley & Sons, 2011.
[2] A. Zukauskas, J. Ziugzda, Heat Transfer of a Cylinder in Crossflow, Hemisphere Publishing Corp., Washington, DC, 1985, p. 219. Translation 1.
[3] R. Nijsing, Temperature and heat flux distribution in nuclear fuel element rods: A calculation of effects due to non-uniform distribution of heat generation, heat transfer coefficient and fuel-cladding contact resistance, Nuclear Eng. Design 4 (1) (1966) 1–20.
[4] D.Q. Kern, A.D. Kraus, Extended Surface Heat Transfer, McGraw Hill, 1972. Available from: <http://books.google.com/books/about/Extended_surface_heat_transfer.html?id=5NpSAAAAMAAJ>.
[5] H.C. Ünal, Determination of the temperature distribution in an extended surface with a non-uniform heat transfer coefficient, Int. J. Heat Mass Transfer 28 (12) (1985) 2279–2284.
[6] H. Barrow, Theoretical solution for the temperature in a straight fin with variable surface heat transfer coefficient, J. Heat Recovery Syst. 6 (6) (1986) 465–468.
[7] S.W. Ma, A.I. Behbahani, Y.G. Tsuei, Two-dimensional rectangular fin with variable heat transfer coefficient, Int. J. Heat Mass Transfer 34 (1) (1991) 79–85.
[8] B. Vick, R.G. Wells, Laminar flow with an axially varying heat transfer coefficient, Int. J. Heat Mass Transfer 29 (12) (1986) 1881–1889.
[9] B. Kundu, P.K. Das, Performance analysis and optimization of straight taper fins with variable heat transfer coefficient, Int. J. Heat Mass Transfer 45 (24) (2002) 4739–4751.
[10] E. Mokheimer, Performance of annular fins with different profiles subject to variable heat transfer coefficient, Int. J. Heat Mass Transfer 45 (17) (2002) 3631–3642.
[11] A.G. Agwu Nnanna, A. Haji-Sheikh, D. Agonafer, Effect of variable heat transfer coefficient, fin geometry, and curvature on the thermal performance of extended surfaces, J. Electron. Packag. 125 (3) (2003) 456–460.
[12] H.L. Lee, H.M. Chou, Y.C. Yang, The function estimation in predicting heat flux of pin fins with variable heat transfer coefficients, Energy Convers. Manage. 45 (11) (2004) 1749–1758.
[13] J. Taler, Determination of local heat transfer coefficient from the solution of the inverse heat conduction problem, Forsch. Ingenieurwes. 71 (2) (2007) 69–78.
[14] H.L. Lee, Y.C. Yang, S.S. Chu, Transient thermoelastic analysis of an annular fin with coupling effect and variable heat transfer coefficient, J. Therm. Stresses 25 (12) (2002) 1105–1120.
[15] Ş. Özgür Atayılmaz, Experimental and numerical study of natural convection heat transfer from horizontal concentric cylinders, Int. J. Therm. Sci. 50 (8) (2011) 1472–1483.
[16] S.J. Drake, D.A. Wetz, J.K. Ostanek, S.P. Miller, J.M. Heinzel, A. Jain, Measurement of anisotropic thermophysical properties of cylindrical Li-ion cells, J. Power Sources 252 (2014) 298–304.
[17] T.M. Bandhauer, S. Garimella, T. Fuller, A critical review of thermal issues in lithium-ion batteries, J. Electrochem. Soc. 158 (2011) R1–R25.
[18] D. Lisbona, T. Snee, A review of hazards associated with primary lithium and lithium-ion batteries, Process Saf. Environ. Prot. 89 (2011) 434–442.
[19] M.N. Ozisik, Heat Conduction, John Wiley & Sons, 1980.